

Spectral decomposition of seismic data with continuous-wavelet transform

Satish Sinha¹, Partha S. Routh², Phil D. Anno³, and John P. Castagna¹

ABSTRACT

This paper presents a new methodology for computing a time-frequency map for nonstationary signals using the continuous-wavelet transform (CWT). The conventional method of producing a time-frequency map using the short time Fourier transform (STFT) limits time-frequency resolution by a predefined window length. In contrast, the CWT method does not require preselecting a window length and does not have a fixed time-frequency resolution over the time-frequency space. CWT uses dilation and translation of a wavelet to produce a time-scale map. A single scale encompasses a frequency band and is inversely proportional to the time support of the dilated wavelet.

Previous workers have converted a time-scale map into a time-frequency map by taking the center frequencies of each scale. We transform the time-scale map by taking the Fourier transform of the inverse CWT to produce a time-frequency map. Thus, a time-scale map is converted into a time-frequency map in which the amplitudes of individual frequencies rather than frequency bands are represented. We refer to such a map as the time-frequency CWT (TFCWT).

We validate our approach with a nonstationary synthetic example and compare the results with the STFT and a typical CWT spectrum. Two field examples illustrate that the TFCWT potentially can be used to detect frequency shadows caused by hydrocarbons and to identify subtle stratigraphic features for reservoir characterization.

(also called spectral decomposition) of a seismic signal aims to characterize the time-dependent frequency response of subsurface rocks and reservoirs. Castagna et al. (2003) use matching-pursuit decomposition for instantaneous spectral analysis to detect low-frequency shadows beneath hydrocarbon reservoirs. A case history of using spectral decomposition and coherency to interpret incised valleys is shown by Peyton et al. (1998). Partyka et al. (1999) use windowed spectral analysis to produce discrete-frequency energy cubes for applications in reservoir characterization. Hardy et al. (2003) show that an average frequency attribute produced from sine curve-fitting strongly correlates with shale volume in a particular area.

Since time-frequency mapping is a nonunique process, various methods exist for time-frequency analysis of nonstationary signals. Jones and Baraniuk (1995) describe a data-adaptive method. The widely used short-time Fourier transform (STFT) method produces a time-frequency spectrum by taking the Fourier transform over a chosen time window (Cohen, 1995). In STFT, time-frequency resolution is fixed over the entire time-frequency space by preselecting a window length. Therefore, resolution in seismic data analysis becomes dependent on a user-specified window length.

Over the past two decades, the wavelet transform has been applied in many branches of science and engineering. The continuous-wavelet transform (CWT) provides a different approach to time-frequency analysis. Instead of producing a time-frequency spectrum, it produces a time-scale map called a scalogram (Rioul and Vetterli, 1991). Since scale represents a frequency band, it is not intuitive if we wish to interpret the frequency content of the signal. Some workers (Hlawatsch and Boudreaux-Bartels, 1992; Abry et al., 1993) take scale to be inversely proportional to the center frequency of the wavelet and represented the scalogram as a time-frequency map.

This paper provides a novel approach for mapping the time-scale map into a time-frequency map. Time-frequency CWT (TFCWT; Sinha, 2002) analysis provides high-frequency

INTRODUCTION

Seismic data, being nonstationary in nature, have varying frequency content in time. Time-frequency decomposition

Manuscript received by the Editor October 21, 2003; revised manuscript received March 15, 2005; published online October 12, 2005.

¹University of Oklahoma, School of Geology and Geophysics, 100 E. Boyd St., 810 SEC, Norman, Oklahoma 73019. E-mail: satish@ou.edu; jcastagnaou@yahoo.com.

²Boise State University, Department of Geosciences, Boise, Idaho 83725. E-mail: prouth@boisestate.edu.

³ConocoPhillips, Seismic Imaging and Prediction, 600 N. Dairy Ashford, Houston, Texas 77252-2197. E-mail: phil.d.anno@conocophillips.com.

© 2005 Society of Exploration Geophysicists. All rights reserved.

resolution at low frequencies and high time resolution at high frequencies. This optimal time-frequency resolution property of the TFCWT makes it useful in seismic data analysis.

Computing the TFCWT in the Fourier domain is a fast process. Furthermore, TFCWT is an invertible process such that the inverse Fourier transform of the time summation of the TFCWT reconstructs the original signal, provided the inverse wavelet transform exists. For our purposes we require only the forward transform; reproducibility is not a strict requirement.

Seismic data analysts sometimes observe low-frequency shadows in association with hydrocarbon reservoirs. The shadow is probably caused by attenuation of high-frequency energy in the reservoir itself (Dilay and Eastwood, 1995; Mitchell et al., 1997), such that the local dominant frequency

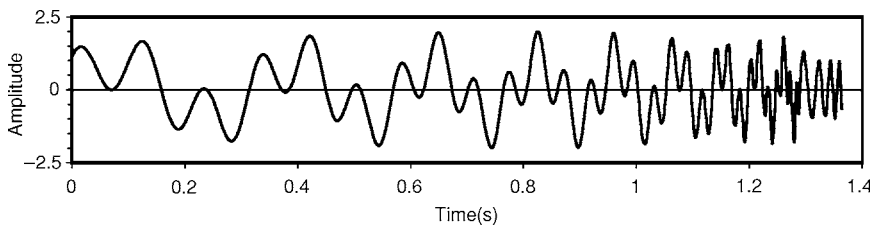


Figure 1. A chirp signal consisting of two known hyperbolic sweep frequencies with constant amplitude for each frequency.

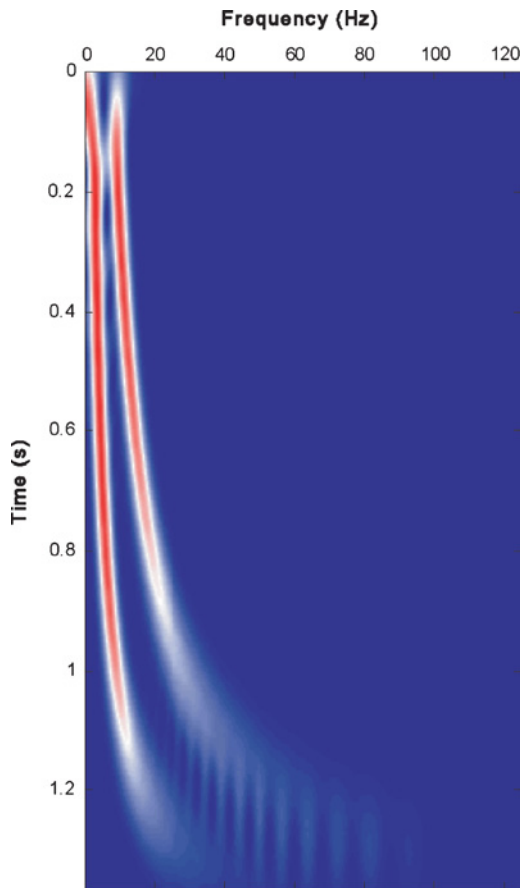


Figure 2. A spectrogram of the chirp signal using a 400-ms window length. Notice that the lower frequencies are well resolved but the higher frequencies are not resolved.

moves toward the low-frequency range. Thus, anomalous low-frequency energy is concentrated at or beneath the reservoir level. The low frequencies are probably not caused by inelastic attenuation. Ebrom (2004) lists about ten possible mechanisms. High-frequency resolution at low frequencies, given by the TFCWT, helps detect these shadows. On the other hand, high time resolution at high frequencies can enhance stratigraphic features from seismic data. Marfurt and Kirlin (2001) investigate how tuning frequency varies with thickness and use spectrally decomposed data to resolve thin beds.

In this paper, we derive a formula to convert a scalogram to a TFCWT. We begin by comparing the TFCWT spectrum for a hyperbolic chirp signal with the CWT spectrum and the STFT. Then we calculate TFCWT spectra for two real data sets, one from Nigeria and another publicly available from the Stratton field, south Texas. In the first example, we show that single-frequency visualization of a seismic section in the frequency domain with the TFCWT reveals low-frequency anomalies associated with hydrocarbon reservoirs. In the second example, we show that single-frequency slices along a horizon can be used to enhance stratigraphic features.

TIME-FREQUENCY MAP FROM STFT

The Fourier transform $\hat{f}(\omega)$ of a signal $f(t)$ is the inner product of the signal with the basis function $e^{i\omega t}$, i.e.,

$$\hat{f}(\omega) = \langle f(t), e^{i\omega t} \rangle = \int_{-\infty}^{\infty} f(t)e^{-i\omega t} dt, \quad (1)$$

where t is time. A seismic signal, when transformed into the frequency domain using the Fourier transform, gives the overall frequency behavior; such a transformation is inadequate for analyzing a nonstationary signal. We can include the time dependence by windowing the signal (i.e., taking short segments of the signal) and then performing the Fourier transform on the windowed data to obtain local frequency information. Such an approach of time-frequency analysis is called the short-time Fourier transform (STFT), and the time-frequency map is called a spectrogram (Cohen, 1995). The STFT is given by the inner product of the signal $f(t)$ with a time-shifted window function $\phi(t)$. Mathematically, it can be expressed as

$$\begin{aligned} STFT(\omega, \tau) &= \langle f(t), \phi(t - \tau)e^{i\omega t} \rangle \\ &= \int_{-\infty}^{\infty} f(t)\bar{\phi}(t - \tau)e^{-i\omega t} dt, \end{aligned} \quad (2)$$

where the window function ϕ is centered at time $t = \tau$, with τ being the translation parameter, and $\bar{\phi}$ is the complex conjugate of ϕ .

We show a spectrogram computed for a chirp signal (Figure 1) with two hyperbolic frequency sweeps in Figure 2. We use a 400-ms-long Hanning window for this computation. Note in the spectrogram that the low frequencies are well resolved and the high frequencies are either poorly resolved or not visible at all. The reason is because the frequency resolution is

fixed by the preselected window length and is recognized as the fundamental problem of the STFT in spectral analysis of a nonstationary signal.

TIME-FREQUENCY MAP FROM CWT (TFCWT)

The CWT is an alternative method to analyze a signal. In the CWT, wavelets dilate in such a way that the time support changes for different frequencies. Smaller time support increases the frequency support, which shifts toward higher frequencies. Similarly, larger time support decreases the frequency support, which shifts toward lower frequencies. Thus, when the time resolution increases, the frequency resolution decreases, and vice versa (Mallat, 1999).

A wavelet is defined as a function $\psi(t) \in L^2(\mathfrak{R})$ with a zero mean, localized in both time and frequency. By dilating and translating this wavelet $\psi(t)$, we produce a family of wavelets:

$$\psi_{\sigma,\tau}(t) = \frac{1}{\sqrt{\sigma}} \psi\left(\frac{t-\tau}{\sigma}\right), \quad (3)$$

where $\sigma, \tau \in \mathfrak{R}$ and σ is not zero and σ is the dilation parameter or scale. Note that the wavelet is normalized such that the L2-norm $\|\psi\|$ is equal to unity. The CWT is defined as the inner product of the family of wavelets $\psi_{\sigma,\tau}(t)$ with the signal $f(t)$. This is given by

$$F_W(\sigma, \tau) = \langle f(t), \psi_{\sigma,\tau}(t) \rangle = \int_{-\infty}^{\infty} f(t) \frac{1}{\sqrt{\sigma}} \bar{\psi}\left(\frac{t-\tau}{\sigma}\right) dt, \quad (4)$$

where $\bar{\psi}$ is the complex conjugate of ψ and $F_W(\sigma, \tau)$ is the time-scale map (i.e., the scalogram). The convolution integral in equation 4 can be computed easily in the Fourier domain. The choice for the scale and the translation parameter can be arbitrary, and we can choose to represent it any way we like. To reconstruct the function $f(t)$ from the wavelet transform, we use Calderon's identity (Daubechies, 1992), given by

$$f(t) = \frac{1}{C_\psi} \int_{-\infty}^{\infty} \int_{-\infty}^{\infty} F_W(\sigma, \tau) \psi\left(\frac{t-\tau}{\sigma}\right) \frac{d\sigma}{\sigma^2} \frac{d\tau}{\sqrt{\sigma}}. \quad (5)$$

For the inverse transform to exist, we require that the analyzing wavelet satisfy the admissibility condition, given by

$$C_\psi = 2\pi \int_{-\infty}^{\infty} \frac{|\hat{\psi}(\omega)|^2}{\omega} d\omega < \infty, \quad (6)$$

where $\hat{\psi}(\omega)$ is the Fourier transform of $\psi(t)$ and where C_ψ is a constant for wavelet ψ . The integrand in equation 6 has an integrable discontinuity at $\omega = 0$ and also implies that $\int \psi(t) dt = 0$. A commonly used wavelet in continuous-wavelet transform is the Morlet wavelet, defined as (Torrence and Compo, 1998)

$$\psi_0(t) = \pi^{-1/4} e^{i\omega_0 t} e^{-t^2/2}, \quad (7)$$

where ω_0 is the frequency and is taken as 2π to satisfy the admissibility condition. The center frequency of the Morlet wavelet being inversely proportional to the scale provides an easy interpretation from scale to frequency.

We note that a scale represents a frequency band and not a single frequency. The scalogram does not provide a direct intuitive interpretation of frequency. To interpret the

time-scale map, in terms of a time-frequency map, a number of approaches can be taken. The easiest step would be to stretch the scale to an equivalent frequency, depending on the scale-frequency mapping of the wavelet. Typically for time-frequency analysis, one converts a scalogram to a time-frequency spectrum using f_c/f , where, f_c is the center frequency of the wavelet (Hlawatsch and Bartels, 1992). Such a typical CWT spectrum of the chirp signal using the Morlet wavelet is shown in Figure 3. However, we take an alternative approach and compute a frequency spectrum of the signal using the wavelet as an adaptive window. Because of the Morlet wavelet's dilation property, it is a natural window for signals that require high-frequency resolution at low frequencies and high time resolution at high frequencies. The translation property allows us to examine the frequency content at various times, thus leading to a time-frequency map that is adaptive to the nonstationary nature of seismic signals. This time-frequency map is obtained by taking the Fourier transform of the inverse continuous wavelet transform.

Replacing $f(t)$ from equation 5 into equation 1 gives

$$\hat{f}(\omega) = \frac{1}{C_\psi} \int_{-\infty}^{\infty} \int_{-\infty}^{\infty} \int_{-\infty}^{\infty} \frac{1}{\sigma^2 \sqrt{\sigma}} \times F_W(\sigma, \tau) \psi\left(\frac{t-\tau}{\sigma}\right) e^{-i\omega t} d\sigma d\tau dt. \quad (8)$$

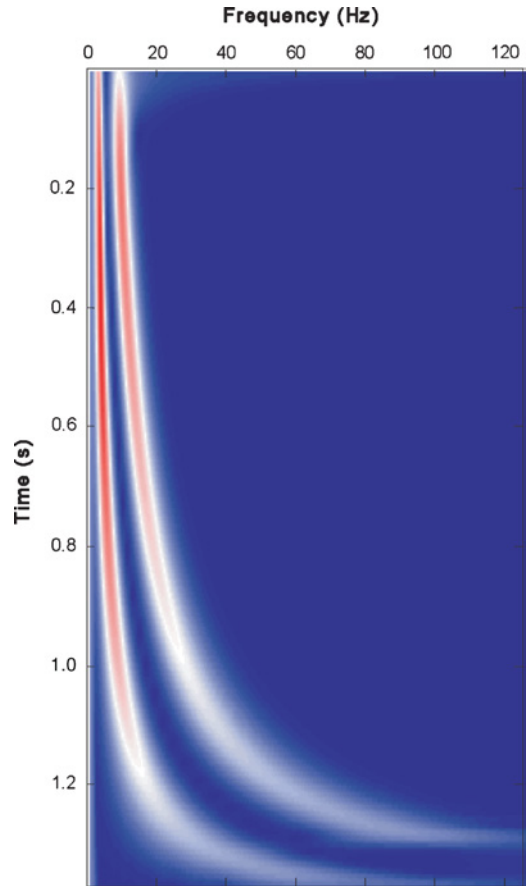


Figure 3. A typical CWT spectrum obtained for the chirp signal shown in Figure 1. It is converted from the scalogram, described by equation (4), using the center frequencies of scales.

Using the scaling and shifting theorem of the Fourier transform, we get

$$\int_{-\infty}^{\infty} \psi \left(\frac{t - \tau}{\sigma} \right) e^{-i\omega t} dt = \sigma e^{-i\omega\tau} \hat{\psi}(\sigma\omega). \quad (9)$$

By interchanging the integrals and substituting equation 9 into equation 8, we obtain

$$\hat{f}(\omega) = \frac{1}{C_\psi} \int_{-\infty}^{\infty} \int_{-\infty}^{\infty} \frac{1}{\sigma^2 \sqrt{\sigma}} F_W(\sigma, \tau) \sigma \hat{\psi}(\sigma\omega) e^{-i\omega\tau} d\sigma d\tau, \quad (10)$$

where $\hat{\psi}(\omega)$ is the Fourier transform of the mother wavelet.

To obtain a time-frequency map, we remove the integration over the translation parameter τ and replace $\hat{f}(\omega)$ by $\hat{f}(\omega, \tau)$. This is given by

$$\hat{f}(\omega, \tau) = \frac{1}{C_\psi} \int_{-\infty}^{\infty} F_W(\sigma, \tau) \hat{\psi}(\sigma\omega) e^{-i\omega\tau} \frac{d\sigma}{\sigma^{3/2}}. \quad (11)$$

Equation 11 is the fundamental equation that allows us to compute TFCWT. This can also be represented as the inner product between the wavelet transform of the signal $F_W(\sigma, \tau)$ and a scaled and modulated window given by $\hat{\psi}_\omega(\sigma)$, where the scaling is over the frequency. For a particular frequency, we have an appropriately scaled window. The integration in the inner product space is over all scales, as denoted by equation 11. This can be represented by

$$\hat{f}(\omega, \tau) = \langle F_W(\sigma, \tau), \hat{\psi}_\omega(\sigma) \rangle, \quad (12)$$

where the scaled and modulated window is given by

$$\hat{\psi}_\omega(\sigma) = \frac{\hat{\psi}(\sigma\omega) e^{-i\omega\tau}}{C_\psi \sigma^{3/2}}. \quad (13)$$

Here, $\bar{\hat{\psi}}_\omega(\sigma)$ is the complex conjugate of $\hat{\psi}_\omega(\sigma)$.

Equation 12 shows that the effective window is the scaled and modulated wavelet that acts on the transformed signal in the wavelet domain. In contrast, the chosen window in the STFT directly operates on the time-domain signal given in equation 2, and the inner product space is integrated over all times. The time-frequency map generated by equation 11 or equation 12 from the scalogram $F_W(\sigma, \tau)$ is not obtained by the direct transformation of a scale to its center frequency; rather, this map provides energy at the desired frequency and avoids the complication of overlapping frequency bands common to a scale-frequency transformation. Equation 11 can be computed using a two-step procedure. First, we evaluate the convolution integral in equation 4 to obtain $F_W(\sigma, \tau)$ using the Fourier transform method. In the second step we use the Fourier transformation of the scaled and modulated wavelet to compute the inner product over all scales. Note that the time summation of equation 11 gives the Fourier transform of the signal. Thus, reconstructing the original signal is a two-step process: (1) time summation of the TFCWT and (2) inverse Fourier transform of the resultant sum.

The synthetic signal (Figure 1) is comprised of two hyperbolic sweep frequencies, each having constant amplitude. In other words, energy in each frequency sweep is constant with time. The typical CWT spectrum (Figure 3) for the synthetic signal improves time-frequency resolution more than

the STFT spectrum (Figure 2). In the CWT spectrum, the energies in both frequency trends erroneously decrease with increasing frequency. Considering the fact that the typical CWT spectrum is computed in terms of frequency bands (i.e., scales) and is represented by taking the center frequency of the frequency bands, these frequency bands overlap each other and the overlap increases with increasing frequency. This results in an apparent loss of energy in the CWT spectrum that can be confused with attenuation effects which are not present in the signal. However, the TFCWT spectrum (Figure 4) does not show any erroneous attenuation. The blurring effect on each end is because the TFCWT has high-frequency resolution and low-time resolution at low frequencies and low-frequency resolution and high time resolution at high frequencies. Thus, the TFCWT improves resolution for a nonstationary signal. In addition to the improvement in the time-frequency resolution, the new methodology inheriting the CWT avoids the subjective choice of window length necessary for the STFT.

APPLICATIONS OF TFCWT TO FIELD DATA

Time-frequency spectra produced from the TFCWT can be used to interpret seismic data in the frequency domain. We have conducted such analyses with poststack data sets. Adding a frequency axis to a 2D seismic section makes the data

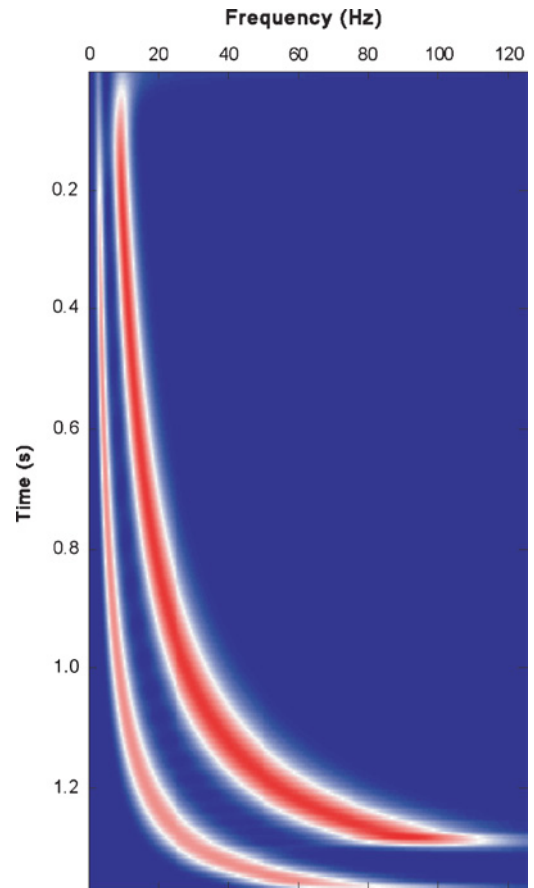


Figure 4. TFCWT spectrum, described by equation 11, obtained for the chirp signal shown in Figure 1 using a complex Morlet wavelet.

three-dimensional. Comparison of single-frequency sections from such a 3D volume can help detect low-frequency shadows sometimes caused by hydrocarbon reservoirs. Sun et al. (2002) use instantaneous spectral analysis based on matching-pursuit decomposition for direct hydrocarbon detection. A matching pursuit isolates the signal structures that are coherent with respect to a given wavelet dictionary (Mallat and Zhang, 1993). However, if the signal is composed of several combinations of fundamental dictionaries, it will be difficult to choose a particular one to analyze the nonstationary nature. In the TFCWT, time-frequency decomposition is carried out by a mother wavelet. This method provides good frequency resolution at low frequencies and is therefore effective in detecting low-frequency shadows.

A seismic section from a Nigeria data set (Figure 5) shows bright amplitudes (yellow arrows) adjacent to faults (green arrows), indicative of known hydrocarbon zones. A preferentially illuminated single-frequency section at 20 Hz from the TFCWT data volume shows high-amplitude, low-frequency

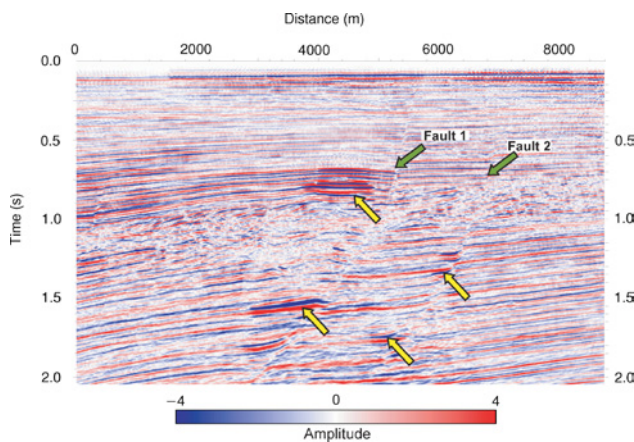


Figure 5. A seismic section from a Nigeria data set. Bright amplitudes indicated by yellow arrows adjacent to the faults (green arrows) in this seismic section are known hydrocarbon zones.

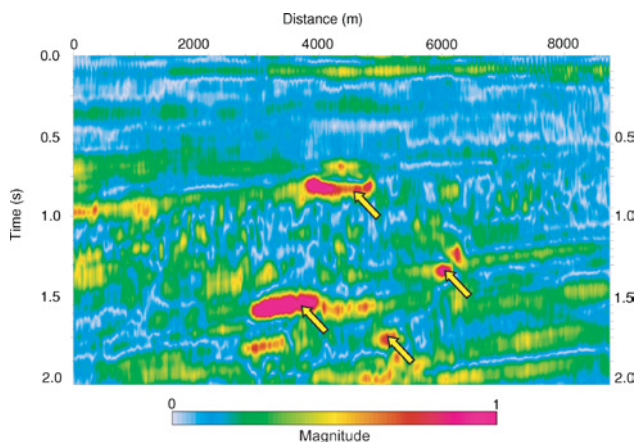


Figure 6. A 20-Hz seismic section obtained using TFCWT processing of the seismic data shown in Figure 5. High-amplitude, low-frequency anomalies (red) are at the hydrocarbon zones (yellow arrows).

anomalies (red) at the reservoir level (yellow arrows) in Figure 6. Furthermore, at 33 Hz these anomalies disappear (Figure 7). In this example these low-frequency anomalies appear only at the known hydrocarbon reservoirs. Mechanisms for this low-frequency anomaly are not known. Ebrom (2004) suggests several possible mechanisms of frequency shadow effect. The challenge is to determine which are first-order effects and which are less important. The anomaly above the hydrocarbon reservoir level (black arrow) in the 33-Hz section is most likely a very thin-bed interference effect that remains anomalous at higher frequencies. This example shows that the comparison of single low-frequency sections from TFCWT has been able to detect low-frequency anomalies caused by hydrocarbons.

We extend this idea to stratigraphic analysis by observing a horizon slice from a 3D volume. Adding a frequency axis to a 3D seismic data volume makes the time-frequency volume 4D and complicates visualization. To simplify visualization, a 3D seismic data volume can be rearranged in two-dimensions according to the trace numbers or CDPs. Time-frequency analysis will extend it in the third dimension, adding a frequency axis to it. From this time-frequency-CDP volume, we can extract a horizon or time slice and rearrange the trace numbers according to their inline and crossline numbers to produce a frequency-space cube [similar to a tuning cube (Partyka et al., 1999)]. Visualizing single-frequency attributes for a horizon from such a 3D cube can be used to identify geologic features that otherwise would not be visible on a usual horizon amplitude map. We utilize the fact that the varying thicknesses tune at varying frequencies. (For details on tuning frequency modeling, see Marfurt and Kirlin, 2001.)

A horizon slice from the Stratton 3D seismic data volume is shown in Figure 8b. This horizon slice is taken 16 ms above the horizon A pick in Figure 8a. A channel, indicated in red, appears to have branches in the middle of the map toward the south. From an interpreter's point of view, knowing the extension of the possible channel is important information for reservoir characterization. A 32-Hz frequency slice for the same horizon slice (Figure 9) shows what could be details of a fluvial-channel system. We observe a pattern similar to that

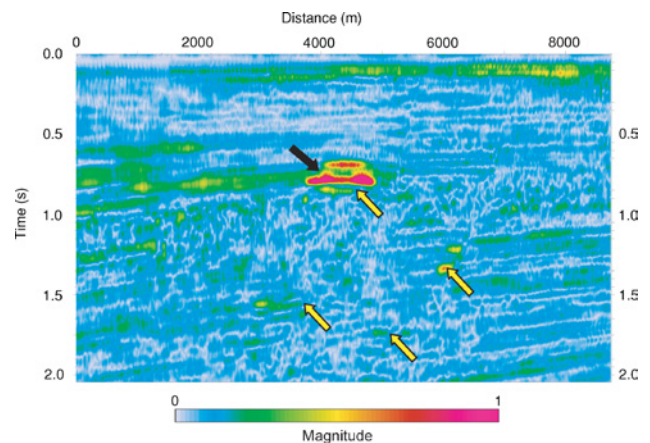


Figure 7. A 33-Hz seismic section of Figure 5 obtained using TFCWT processing. In this section frequency anomalies associated with frequency shadows are absent (yellow arrows). The anomaly (black arrow) present in this section is from local tuning effects and does not disappear at higher frequencies.

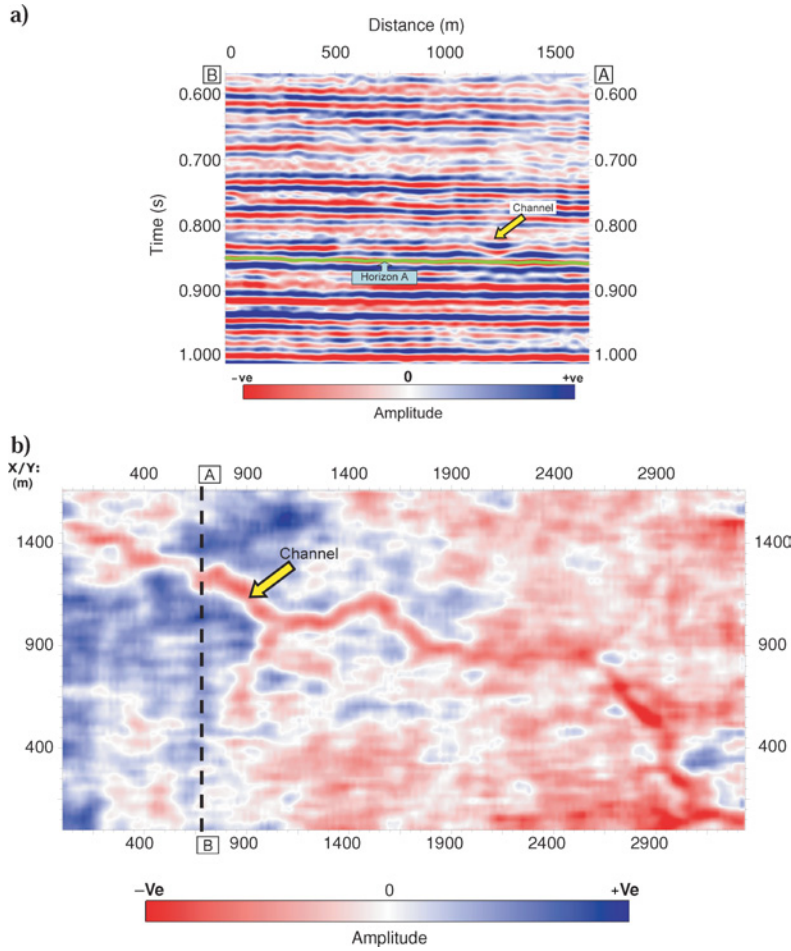


Figure 8. (a) A vertical seismic section through the Stratton 3D data set corresponding to line *AB* shown in (b). (b) A horizon slice through the seismic amplitude volume 16 ms above the horizon *A* pick shown in (a). A fluvial channel (yellow arrow) shows up as a negative-amplitude trough on the horizon slice and corresponds to the channel shown in (a). The southwestern branch of this channel is not clear.

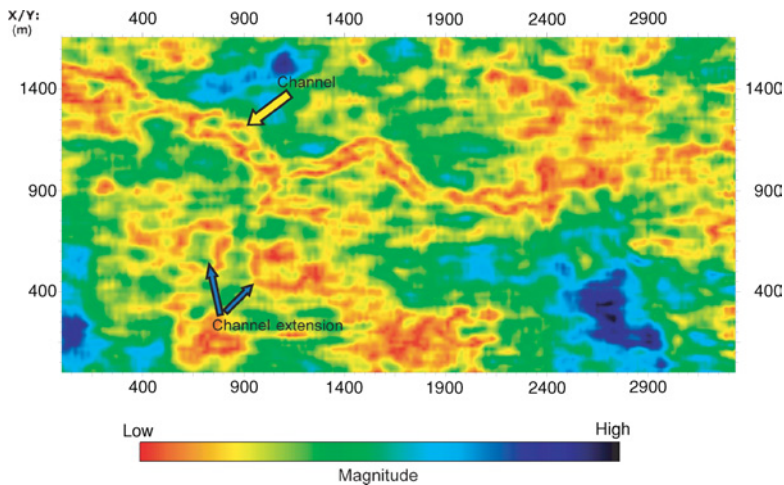


Figure 9. A horizon slice at 32 Hz through the TFCWT volume corresponding to the seismic-amplitude map shown in Figure 8b. Note the channel extension (blue arrows) and internal heterogeneity of the fluvial-channel system.

of a complex meandering-channel system in the southwestern part of the figure. Also note that the apparent internal heterogeneity of the main fluvial-channel system is enhanced by spectral decomposition. The relatively low spectral amplitude of the channel is indicative of a lithology change (possibly brine-filled sand).

CONCLUSIONS

A conventional method of computing a time-frequency spectrum, or spectrogram, using the STFT method requires a predefined time window and therefore has fixed time-frequency resolution. However, to analyze a nonstationary signal where frequency changes with time, we require a time-varying window. The CWT dilates and compresses wavelets to provide a time-scale spectrum instead of a time-frequency spectrum. Converting a scalogram into a time-frequency spectrum using the center frequency of a scale gives an erroneous attenuation in the spectrum. The TFCWT overcomes this problem and gives a more robust technique of time-frequency localization. Since TFCWT is fundamentally derived from the continuous-wavelet transform, wavelet dilation and compression effectively provides the optimal window length, depending upon the frequency content of the signal. Thus, it eliminates the subjective choice of a window length and provides an optimal time-frequency spectrum without any erroneous attenuation effect for a nonstationary signal. It has high-frequency resolution at low frequencies and high time resolution at high frequencies, whereas the spectrogram has fixed time-frequency resolution throughout.

Thus, in nonstationary seismic data analysis the TFCWT has a natural advantage over the STFT and the typical CWT spectrum. Though STFT allows one to analyze an entire stratigraphic interval, TFCWT is focused on the spectral attributes of horizons rather than intervals. STFT may be more efficient for estimating the spectral characteristics of long intervals as compared to the support of the CWT. However, TFCWT can be summed over time to resolve the spectrum of any desired interval. The field examples on single-frequency sections and maps from the TFCWT presented in this work suggest that such analysis potentially can be used as direct hydrocarbon indicators and for improved stratigraphic visualization.

ACKNOWLEDGMENTS

The authors acknowledge the Conoco research scientists for their valuable input. They would also like to thank Conoco (now ConocoPhillips) for providing a field-data set and logistical support for this research and particularly Dale Cox of Conoco for many useful discussions

and help in the practical implementation in SeismicUnix (SU). The authors are grateful to the Shell Crustal Imaging Facility at the University of Oklahoma for software support. Finally, the authors thank Kurt Marfurt, the associate editor of *Geophysics*, and two reviewers for their valuable comments and suggestions.

REFERENCES

- Abry, P., P. Goncalves, and P. Flandrin, 1993, Wavelet-based spectral analysis of $1/f$ processes: International Conference on Acoustic, Speech and Signal Processing, IEEE, Proceedings, **3**, 237–240.
- Castagna, J. P., S. Sun, and R. W. Seigfried, 2003, Instantaneous spectral analysis: Detection of low-frequency shadows associated with hydrocarbons: *The Leading Edge*, **22**, 120–127.
- Cohen, L., 1995, *Time-frequency analysis*: Prentice Hall, Inc.
- Daubechies, I., 1992, *Ten lectures on wavelets*: Society of Industrial and Applied Mathematics.
- Dilay, A., and J. Eastwood, 1995, Spectral analysis applied to seismic monitoring of thermal recovery: *The Leading Edge*, **14**, 1117–1122.
- Ebrom, D., 2004, The low frequency gas shadows in seismic sections: *The Leading Edge*, **23**, 772.
- Hardy, H. H., A. B. Richard, and J. D. Gaston, 2003, Frequency estimates of seismic traces: *Geophysics*, **68**, 370–380.
- Hlawatsch, F., and G. F. Boudreaux-Bartels, 1992, Linear and quadratic time-frequency signal representations: *IEEE Signal Processing*, **9**, no. 2, 21–67.
- Jones, D. L., and R. G. Baraniuk, 1995, An adaptive optimal-kernel time-frequency representation: *IEEE Transactions on Signal Processing*, **43**, 2361–2371.
- Mallat, S., 1999, *A wavelet tour of signal processing*, 2nd ed.: Academic Press Inc.
- Mallat, S., and Z. Zhang, 1993, Matching pursuits with time-frequency dictionaries: *IEEE Transactions on Signal Processing*, **41**, 3397–3415.
- Marfurt, K. J., and R. L. Kirilin, 2001, Narrow-band spectral analysis and thin-bed tuning: *Geophysics*, **66**, 1274–1283.
- Mitchell, J. T., N. Derzhi, and E. Lickman, 1997, Low frequency shadows: The rule, or the exception? 67th Annual International Meeting, SEG, Expanded Abstracts, 685–686.
- Partyka, G., J. Gridley, and J. Lopez, 1999, Interpretational applications of spectral decomposition in reservoir characterization: *The Leading Edge*, **18**, 353–360.
- Peyton, L., R. Bottjer, and G. Partyka, 1998, Interpretation of incised valleys using new 3-D seismic techniques: A case history using spectral decomposition and coherency: *The Leading Edge*, **17**, 1294–1298.
- Rioul, O., and M. Vetterli, 1991, Wavelets and signal processing: *IEEE Signal Processing*, **8**, no. 4, 14–38.
- Sinha, S., 2002, *Time-frequency localization with wavelet transform and its application in seismic data analysis*: M.S. thesis, University of Oklahoma.
- Sun, S., J. P. Castagna, and R. W. Seigfried, 2002, Examples of wavelet transform time-frequency analysis in direct hydrocarbon detection: 72nd Annual International Meeting, SEG, Expanded Abstracts, 457–460.
- Torrence, C., and G. P. Compo, 1998, A practical guide to wavelet analysis: *Bulletin of the American Meteorological Society*, **79**, no. 1, 61–78.